Indonesian Journal of Maritime Technology (ISMATECH)
Vol. 04, Issue 01, June 2026
eISSN: 3025-518X
DOI: https://doi.org/10.35718/ismatech.v4i1.8481967

Development of Practical Wind-Assisted Ship Propulsion (WASP) Calculations for Fuel Consumption and Emission Reduction

Isna Aulia Marifa[1], Dian Purnama Sari[2], Wiwin Sulistyawati[1*]

[1]Department of Naval Engineering, Universitas Pembangunan Nasional Veteran Jakarta, Jl. R.S Fatmawati No. 1, Cilandak, Jakarta Selatan, 12450, Indonesia
[2]Research Center for Hydrodynamic Technology, National Research and Innovation Agency, Jl. Hidro Dinamika, Keputih, Kec. Sukolilo, Surabaya, Jawa Timur, 60117, Indonesia

KEYWORDS
Wind Assisted Ship Propulsion;
Route Optimization;
Energy Efficiency;
Carbon Emissions.

ABSTRACT – Integration of Wind-Assisted Ship Propulsion (WASP) serves as a strategic solution for the maritime industry to achieve Net Zero Emission by 2050. This research evaluated the interaction between sail design and route optimization for a 265 GT fishing vessel operating around Benoa, Bali to maximize fuel savings and emission reductions. Three hard sail profiles, arc-shaped, NACA 0012, and NACA 0015, were analyzed at operational speeds of 7 and 10 knots. An improved weather-routing framework based on the A* (A-star) algorithm* was developed, integrating weather forecasts, ship specifications, and force matrices to determine optimal navigational paths. Simulations conducted on routes around Benoa, Bali, demonstrated that the combination of aerodynamic wing sails and intelligent routing improved efficiency by 1.24% to 12.59%. The results confirmed that the synergy between WASP technology and precise pathfinding significantly reduced carbon footprints while enhancing the economic viability of shipping operations. These findings provide a scalable framework for sustainable maritime practices and for achieving global decarbonization targets.

*Corresponding Author | Wiwin Sulistywati | ✉ (wiwinsulistyawati@upnvj.ac.id)

INTRODUCTION

The shipping industry is responsible for moving approximately 90% of the world's traded goods by tonnage. Data shows that between 1970 and 2013, the annual loaded shipping tonnage surged from 2.6 billion to 9.5 billion tons [1]. While this growth drives global trade, it also puts the sector under heavy scrutiny for its contribution to greenhouse gas emissions and air pollution. To address this, the International Maritime Organization (IMO) has set a clear target: achieving Net Zero Emissions by 2050 [2]. Reducing the environmental impact of shipping, which currently accounts for 2-3% of global carbon emissions, has now become a central priority in modern ship design and operations.

Meeting these IMO targets requires a shift toward energy efficiency and renewable sources, such as wind power [2]. Various research innovations have been developed to support decarbonization in the maritime sector. Among them, biodiesel derived from vegetable oils and waste cooking oil (WCO) has shown promising results in reducing exhaust emissions and improving environmental performance [3], [4]. However, further treatment and optimization are still required to achieve engine performance comparable to conventional hydrocarbon fuels. In parallel, alternative approaches focusing on energy-saving technologies have gained attention, particularly the development of Wind-Assisted Ship Propulsion (WASP) systems [5], [6], which are expected to play a significant role in enhancing the sustainability and environmental performance of modern shipping.

The effectiveness of any WASP system depends heavily on wind speed and direction. For a 199-meter vessel, optimal performance is typically found at wind speeds around 10 m/s [6]. While wind direction is a standard reference in route planning, WASP systems work best when paired with route optimization that reacts to real-time environmental conditions. The goal of this optimization is straightforward: minimize operational costs, cut fuel consumption, and lower shipping risks [7].

A previous study [6] on Very Large Crude Carriers (VLCC) highlighted that integrating WASP with route and speed optimization can reduce fuel consumption by up to 80.37% compared to normal operations. Even though this increased travel time to 101.9% of the norm, the trade-off was highly beneficial, given the massive reduction in carbon emissions (78.63% of conventional levels).

However, there is still a lack of comparative research on how different sail shapes, specifically arc-shaped versus specialized NACA airfoils, interact with routing algorithms on specific regional routes. To fill this gap, this study evaluates three sail designs (arc-shaped, NACA 0012, and NACA 0015) using an improved weather routing framework based on the A* (A-star) algorithm. By simulating routes around Benoa, Bali, and testing

operational speeds of 7 and 10 knots, this research integrates force matrices and weather forecasts to find the most efficient setup. This study compares advanced sail geometries under realistic routing scenarios and introduces a practical decision-making framework an approach not previously applied to small-scale fishing vessels in Indonesian waters. Through this framework, the work aims to demonstrate that WASP is a practical, high-impact technology capable of advancing both environmental and economic goals in the maritime sector.

METHODS

This study uses a 265 GT sample ship sailing from Benoa to Bali, as this is the common route among local fishermen. The 265 GT fishing vessel used as the research object has the specifications listed in Table 1.

Table 1. Fishing Hull Specification.

Dimension	Notation	Value
Length Overall (m)	L_{OA}	33.50
Length Between Perpendicular (m)	L_{BP}	29.05
Beam (m)	B	7.95
Height (m)	H	6.02
Draught (m)	T	2.59

The following are the types and sizes of wing sails listed in Table 2.

Table 2. Parameter of Sail.

Dimension	Notation	Value
Sail Area (m^2)	S	20.80

Based on the provided data, the following diagram presents the Coefficient of Lift (CL) for the three airfoil designs across the Angle of Attack (α) range of 0° to 90°. The aerodynamic performance data (sail characteristics) for these three airfoils were adopted from existing literature [9] - [11]. The aerodynamic forces acting on the airfoil are analyzed over the operational angle of attack range of 0° to 20°.

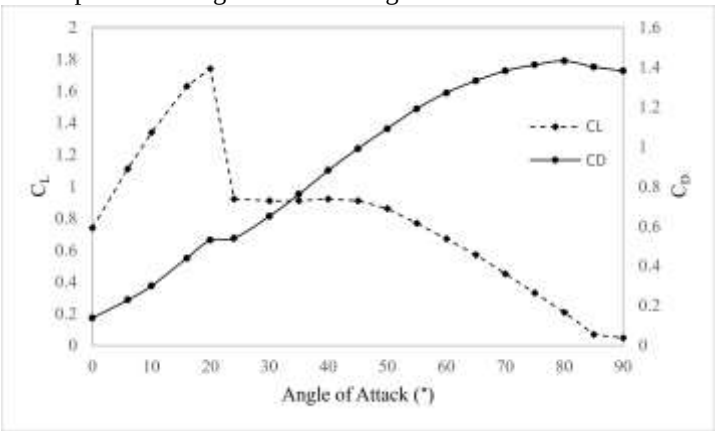

Figure 1. Aerodynamic Properties of Airfoil Arc-Shaped

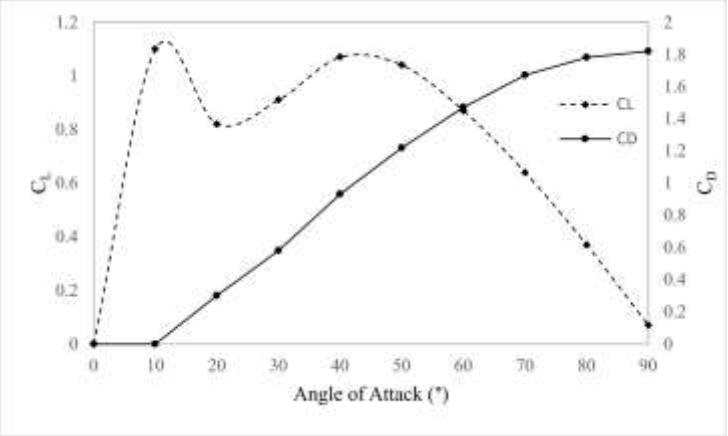

Figure 2. Aerodynamic Properties of Airfoil NACA 0012

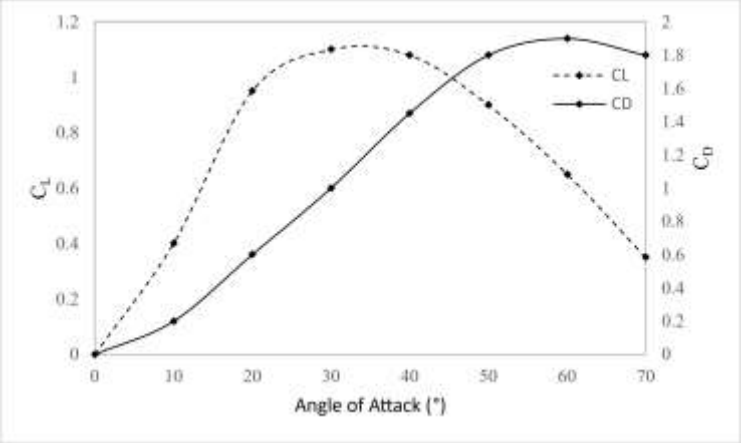

Figure 3. Aerodynamic Properties of Airfoil NACA 0015

Wing sails are developed as auxiliary driving power for hybrid ships. Its main purpose is to reduce fuel consumption and CO_2 emissions. 3 wing-sail shapes are used in this study: arc-shaped, NACA 0012, and NACA 0015. While the arc-shaped wing sail is not common, it has been developed through aerodynamic optimization using the PARSEC wing profile parameterization method and the PSO (Particle Swarm Optimization) algorithm. This optimization has been proven to provide better aerodynamic characteristics than traditional designs [9].

The following are the specifications of the ship's engine listed in Table 3.

Table 3. Specifications of the Ship's Engine

Dimension	Notation
Brand and Type of Main Engine	MITSUBISHI S6R2MPTK
Power (kW)	530
Specific Fuel Oil Consumption (g/kWh)	207

NACA 0012 and NACA 0015 are industry-standard four-digit symmetric airfoil profiles, denoted by the "00" code, which signifies zero camber. Due to their symmetric geometry, both fail to generate lift (CL=0) at a zero Angle of Attack (α=0∘), resulting in no significant changes observed in their aerodynamic characteristics [12]. The primary difference is the maximum thickness-to-chord length ratio, 12% for the NACA 0012 (often used as a comparative benchmark) and 15% for the NACA 0015 (commonly used in wind turbine blades and vertical stabilizers) [13].

Route

Fundamental data on fishing vessel movements are obtained comprehensively from the Vessel Monitoring System (VMS). This VMS data collection is crucial because it accurately records the position and time of each registered vessel, enabling historical tracking of activities.

Furthermore, the raw data is analyzed in depth to identify and map routine and repetitive vessel movement patterns. This analysis specifically focuses on the transitions or journeys made by vessels from their point of departure, namely the fishing port, to their destination fishing grounds. Based on extensive movement pattern analysis, three (3) significant main shipping routes have been identified. These three routes have identical departure points, indicating that all vessels depart from the same port, but they then split and head to different fishing destinations.

The specific coordinates for each successfully mapped route are shown in Figures 4, 5, and 6, as follows:

1. Route 1: Starting from coordinates (115.258°, -8.835°) and ending at the fishing area located at (114.103°, -14.667°), this is the shortest route.
2. Route 2: Departing from the same point (115.258°, -8.835°) but heading to the furthest fishing destination with coordinates (102.156°, -18.436°).
3. Route 3: Starts from (115.258°, -8.835°) and has a fishing destination located at coordinates (109.311°, -20.669°).

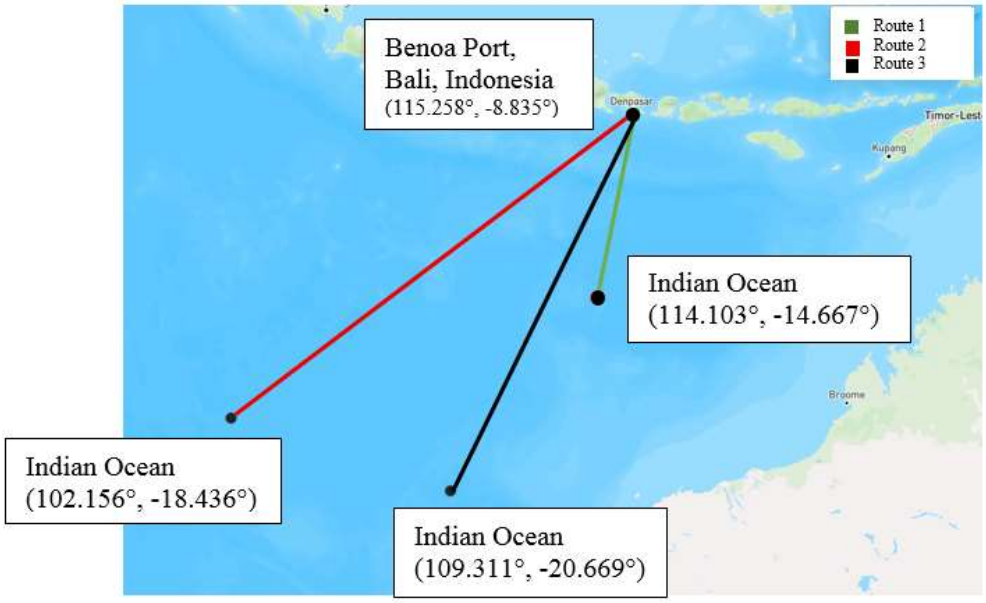

Figure 4. Empirical Route 1

Force Analysis and Mathematical Model of Wing Sail-Assisted Ship

The performance of the sail uses aerodynamic principles through analysis of the lift coefficient (C_L), drag coefficient (C_D), and thrust generated. The aerodynamic forces acting on the sail, in the form of lift coefficient and drag coefficient, were obtained from studies [9] - [11].

$$C_L = \frac{F_L}{\frac{1}{2} \cdot \rho \cdot AWS^2 \cdot S} \tag{1}$$

Where Coefficient of Lift (CL) is a dimensionless value that quantifies the amount of lift generated by an airfoil or a lifting body. FL (Lift Force) is the actual upward force generated by the airfoil, measured in Newtons (N). ρ is the mass of air per unit volume (kg/m^3). AWS (Apparent Wind Speed) is the velocity of the air flowing over the airfoil (m/s). And S (Surface Area) is the reference area of the lifting surface (m^2). The airflow passing through the airfoil profile creates a speed difference and, in turn, a pressure difference, which ultimately generates a lift force. The resultant of the lift force and friction in the direction of the ship's speed is the propulsive force [14]. The greater the lift force generated, the higher the efficiency.

$$C_D = \frac{F_D}{\frac{1}{2} \cdot \rho \cdot AWS^2 \cdot S} \tag{2}$$

Where Coefficient of Drag (CD) is the aerodynamic force acting parallel and opposite to the direction of the airflow. The lift and the drag coefficient represent different forces, but both coefficients are calculated by dividing the relevant aerodynamic force by the same factor. Conversely, the goal is to minimize the coefficient of drag to reduce fuel consumption and increase speed. A lower CD means less air drag.

$$C_T = c_L \sin(\beta) - C_D \cos(\beta) \tag{3}$$

$$F_{Thrust} = \frac{1}{2} \rho V_A^2 S C_T \tag{4}$$

Where F thrust is the component of the total aerodynamic force vector acting in the direction of the ship's heading. The Angle of Attack (α) is the angle between the sail's chord line and the direction of the apparent wind. By optimizing α, the ship maximizes the sail Lift-to-Drag ratio, which is critical for reducing engine load, improving fuel efficiency, and lowering emissions [15].

Powering Engine Of Ship

Propulsive power is the amount of power required to move a ship and maintain its speed in the water. The following is a derivation for calculating the total power required by a ship to maintain a specified or estimated speed:

$$EHP = R_T \times V_S \tag{5}$$

Where Effective Horsepower (EHP) is a measure of the actual power required to propel a vessel at a given speed against total water resistance (kW). R_T is the total resistance of the ship (N). That includes frictional resistance, form resistance, and wave resistance. The total resistance of the ship is obtained from the speed-power diagram corresponding to the ship's speed. And Vs is the actual ship speed.

$$SHP = \frac{EHP}{\eta P} \tag{6}$$

Where shaft horsepower (kW) is the power transmitted to the propeller shaft, after deducting losses in the gearbox and bearings. This study includes a 15% sea margin. ηP is propulsive efficiency, being a measure of how effectively a propulsion system converts available power into useful power to propel a vehicle forward. SHP was used in this study to calculate the sail's power efficiency.

Model Optimalization

The Great Circle Route is a route determination system for finding the shortest distance between two points. The intermediate points on the shortest route are then calculated between the origin and destination points [16]. In searching for the great-circle route, the A* algorithm is used to find the routing result. The A* algorithm is a very popular graph search algorithm and one of the most widely used. This algorithm is innovative because it successfully combines the precision of the Dijkstra algorithm (formal approach) with the efficiency of Best-First-Search (heuristic approach) to efficiently find the shortest path from start to finish within the available map area. As a graph search algorithm, A* is used to determine an optimal route connecting a specified initial node to a desired objective node [17]. A* is a search and pathfinding algorithm applied to weighted graphs. The most crucial step in using it in any scenario is to define the cost function $\big(g(n)\big)$ and the corresponding heuristic function $\big(h(n)\big)$ to be optimized (minimized). A* selects the best path based on the minimum total cost.

$$f(n) = \mathrm{g}(n) + \mathrm{h}(n) \tag{7}$$

Where (g(n)) is the actual path cost from the starting node to node n, and (h(n)) is the lowest estimated cost from node n to the final node [6].

Wind Resource Analysis Method

Data from NASA's Quiescent from Scatterometer Climatology of Ocean Winds (SCOW) are used as a historical sea surface wind climatology derived from satellite-based scatterometer instruments. Advances in satellite-based remote sensing technology have enabled the global acquisition of sea surface wind data with high spatial and temporal consistency. This development opens great opportunities for more detailed and systematic analysis of atmospheric-ocean dynamics in the context of climatology and physical oceanography. One of the key instruments in this advancement is QuikSCAT (Quick Scatterometer). QuikSCAT data provide sea surface wind fields from long-term observations. The SCOW dataset is currently based on 122 months (about 10 years) of QuikSCAT data, covering the period from September 1999 to October 2009, and data collected at a height of 10 meters above sea level. Data have a spatial resolution of 0.25° and a daily temporal resolution (1 day), enabling climatological and ocean wind dynamics analysis at an important level of detail [18]. The shipping routes covered the Benoa-Indian Ocean region, where the port leads to fishing grounds, and three routes were analyzed.

The following are the steps in obtaining wind field information and shipping routes using spatial and temporal interpolation methods:

1. Data Acquisition: collecting wind data that is spatially (latitude and longitude) and temporally (time) dispersed. The A* algorithm is used here to calculate shipping routes that avoid land and to find the shortest path from one point to another, modeling optimization using a great circle.
2. Filtering data for each specific month to prepare data for interpolation
3. Interpolating temporal and spatial data, creating average wind data for the entire month, and predicting or estimating wind speed and direction (wind vectors) at each waypoint.

TFOC and Emission CO_2 Calculation

Marine fuel is an important topic in the maritime industry, particularly amid increasing awareness of environmental impacts and the need for efficiency. Fuel efficiency directly reduces emissions. Based on fuel consumption data, CO_2 emissions for each ship can be estimated. To calculate TFOC efficiency and CO_2 emissions, refer to [19], [20].

$$TFOC = SOFC \times Engine\ power(kW) \times t \quad (8)$$

Where TFOC (Total fuel oil consumption) is calculated as a benchmark to compare the fuel efficiency of fuel saved by the sail during the voyage. The SFOC (Specific Fuel Oil Consumption) value is shown in Table 3. Engine power takes the shaft horsepower value with a sea margin of 15%, and the ship's power without sail is subtracted from the sail power to calculate the TFOC reduction. And the time (hr) is the voyage duration.

$$Emission = TFOC \times EF \quad (9)$$

This calculation uses emission factors (3.114 for CO_2) that correlate fuel consumption with CO_2 output, taking into account the type of fuel used, which is assumed to be Marine Diesel Oil (MDO) [20], [21].

$$\eta = 1 - \frac{F_{WASP}}{F_{ref}} \quad (10)$$

The TFOC reduction (η) is calculated using Equation (10), where (F_{WASP}) represents the fuel oil consumption in the sailing condition using Wind-Assisted Ship Propulsion (WASP), and (F_{ref}) represents the fuel oil consumption of the vessel in its original condition without sails. To ensure the methodology's validity, research simulations and efficiency calculations were conducted on a per-trip basis. This approach enables a more granular analysis of system performance, accounting for significant variations in environmental conditions and operational.

RESULTS AND DISCUSSION

Environmental condition data, including dynamic parameters such as wind speed and wind direction, plays a crucial role as the primary input for analyzing ship performance and voyage efficiency. Specifically, all wind data used in this analysis have been standardized to a reference height of 10 meters above sea level. This 10-meter altitude is internationally recognized as the standard reference in maritime meteorology and oceanography for evaluating and predicting ship performance [22] - [25]. Adherence to this standard is essential, as it ensures an accurate and consistent comparison between the study's findings and historical meteorological records or data from other vessels.

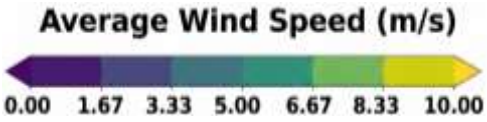

Figure 5. Wind Speed Scale on the Map

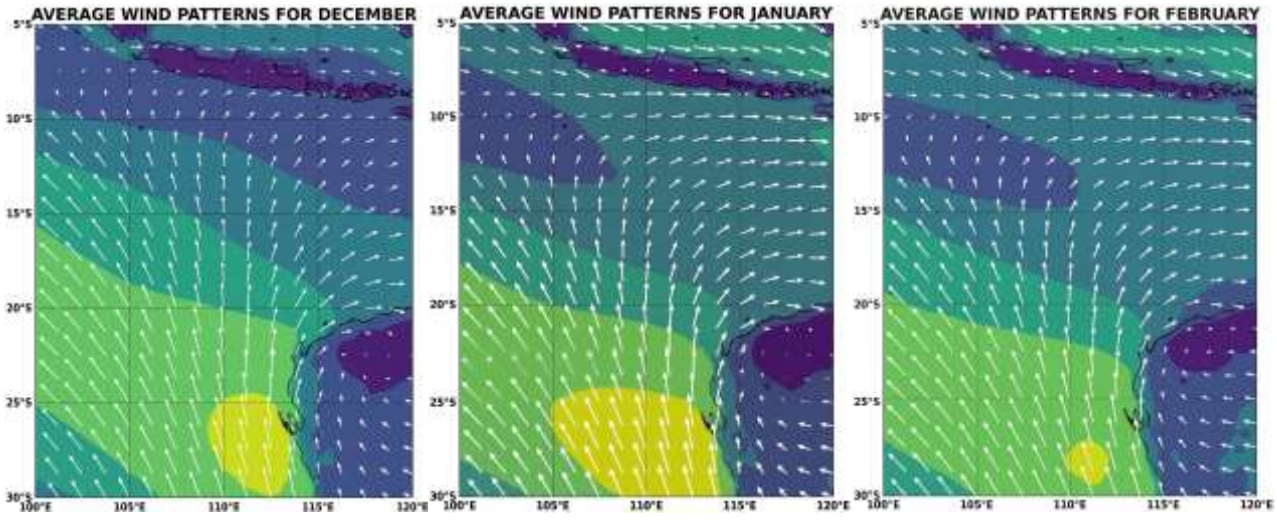

Figure 6. Wind Map of the Sailing Region During the West Monsoon

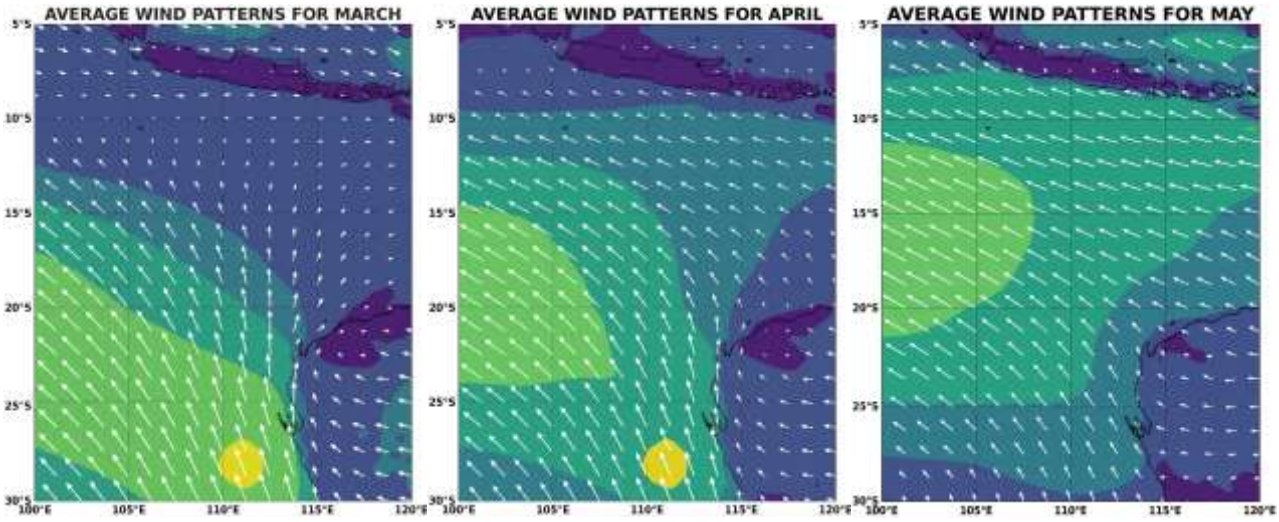

Figure 7. Wind Map of the Sailing Region During the Transition I

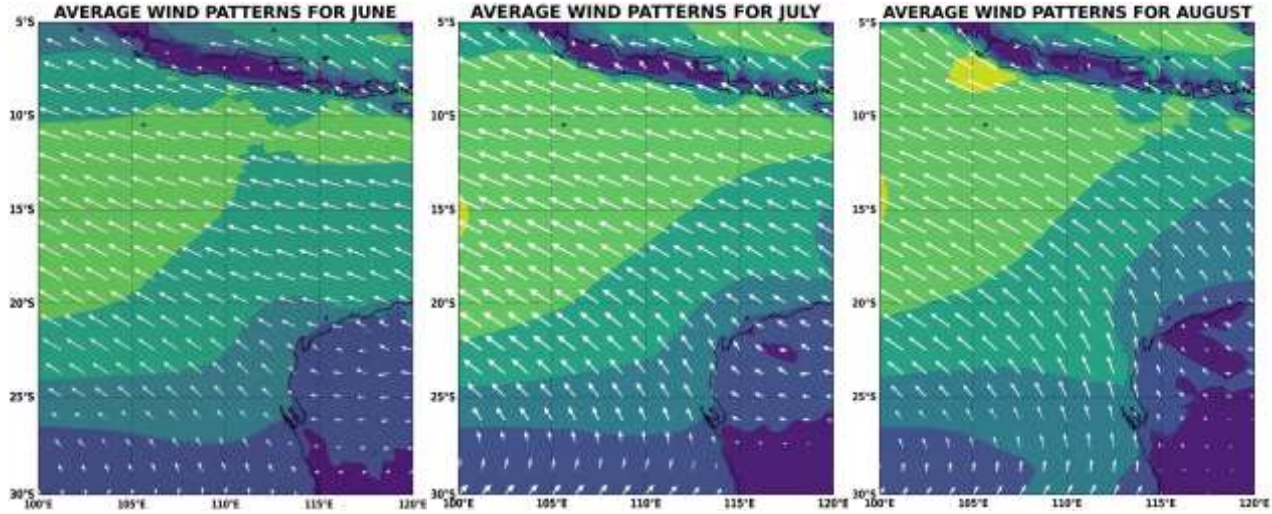

Figure 8. Wind Map of the Sailing Region During the East Monsoon

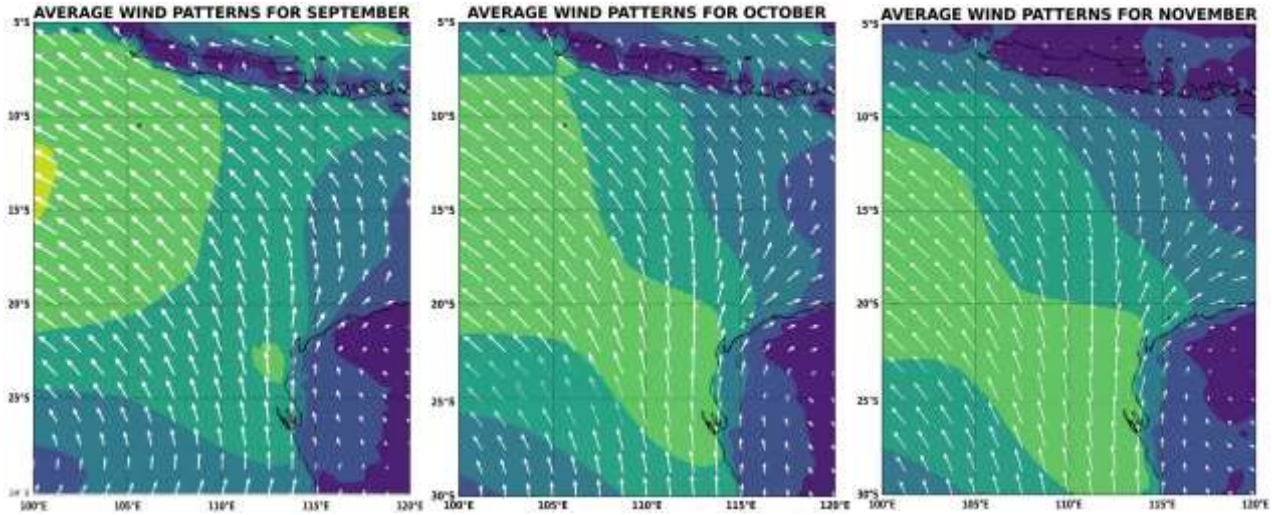

Figure 9. Wind Map of the Sailing Region During the Transition II

Furthermore, in figures 6 through 11, to facilitate quick, intuitive detection and analysis of wind patterns, differences in wind velocity along the sailing route are visualized using a color grid. This visualization serves as a highly effective geospatial diagnostic tool, enabling analysts to rapidly and precisely identify critical areas with

significant variations in wind strength. This capability to map spatial variations is crucial for pinpointing locations that are potentially advantageous or detrimental to the voyage, thereby serving as a key factor in determining the optimal, fuel-efficient sailing route. Wind characteristics in Indonesian waters are predominantly governed by the Asian-Australian monsoon system, inducing significant annual variability in wind speed and direction. This system is periodically categorized into the West Monsoon (December–February), Transition 1 (March–May), East Monsoon (June–August), and Transition 2 (September–November) [26]. A seasonal-based approach provides a more representative assessment of vessel operational effectiveness by accounting for shifts in ocean energy distribution driven by monsoonal cycles. This strategy mitigates potential biases from analyses based solely on extreme parameters that fail to reflect year-round environmental conditions [27].

Great Circle Route Optimization Model Result

The optimization model developed successfully produced highly efficient shipping route solutions, represented as large circular routes. These routes are designed for ships to navigate using the A* algorithm, a method for finding the shortest path that excels in complex, dynamic environments. The resulting map displays route recommendations as colored lines connecting the departure point to various destinations.

The fundamental advantage of this model is its ability to integrate and account for dynamic factors at sea, including currents, waves, and wind speed, which significantly impact ship performance. Therefore, the recommended route is not only the shortest geometric route but also the most efficient and cost-effective, especially in terms of fuel consumption. By prioritizing minimizing operational costs rather than distance traveled, this optimization model offers crucial strategic guidance for modern maritime navigation.

Figure 10. Results of the (GCR) Optimization Model Simulation on Route 1

Figure 11. Results of the (GCR) Optimization Model Simulation on Route 2

Figure 12. Results of the (GCR) Optimization Model Simulation on Route 3

Saving Effect of Wing Sails on Target Route

The two speed points were selected to evaluate how efficiently the propulsion system operates under varying real sea conditions. Mathematical modeling indicates that integrating sail technology can generate an effective thrust of 5.26 kW, significantly improving operational economy with estimated fuel savings of 68.37 liters per voyage. Further validation was conducted by analyzing fuel consumption efficiency and potential emission reductions using parameters in Equation 10. The results show fluctuations in sail system efficiency; however, both peak and minimum values exhibit a consistent pattern along the voyage route. This consistency suggests a strong influence of seasonal cycles on wind energy availability.

Overall, the effectiveness of the wind propulsion system depends on local wind speed and direction dynamics. Consequently, the additional thrust produced by the sail varies with seasonal changes, highlighting the importance of understanding regional wind patterns to optimize vessel performance.

Table 4. Efficiency Results on Route 1 with Arc-shaped Sail

ROUTE 1 (369.14 NM)								
Arc Shaped								
Months	7 Knot (52.73 hr)				10 Knot (36.91 hr)			
	41.79 kW		2203.50 kWh		182.00 kW		6718.35 kWh	
	TFOC w/o sail = 543.00 L Emission w/o sail = 1690.92 kg				TFOC w/o sail = 1655.59 L Emission w/o sail = 5155.52 kg			
	Power Sail (kW)	TFOC w/Sail (L)	Emission (kg)	Reduction (%)	Power Sail (kW)	TFOC w/Sail (L)	Emission (kg)	Reduction (%)
Jan	3.20	501.49	1561.63	7.65	6.47	1596.74	4972.25	3.55
Feb	2.71	507.75	1581.14	6.49	5.66	1604.07	4995.07	3.11
Mar	1.49	523.66	1630.69	3.56	3.80	1621.01	5047.81	2.09
Apr	2.44	511.26	1592.06	5.85	5.19	1608.40	5008.57	2.85
May	4.02	490.77	1528.27	9.62	7.44	1587.91	4944.75	4.09
Jun	4.67	482.27	1501.80	11.18	8.40	1579.15	4917.47	4.62
Jul	5.26	474.63	1478.01	12.59	9.45	1569.60	4887.74	5.19
Aug	5.09	476.81	1484.77	12.19	9.39	1570.22	4889.65	5.16
Sep	4.59	483.43	1505.39	10.97	8.95	1574.16	4901.92	4.92
Oct	3.86	492.90	1534.88	9.23	7.94	1583.40	4930.69	4.36
Nov	3.26	500.59	1558.84	7.81	7.00	1591.96	4957.37	3.84
Dec	2.60	509.27	1585.86	6.21	5.80	1602.83	4991.22	3.19

Table 5. Efficiency Results on Route 2 with Arc-shaped Sail

ROUTE 2 (998.37 NM)								
Arc Shaped								
Months	7 Knot (142.62 hr)				10 Knot (99.84 hr)			
	41.79 kW		5959.64 kWh		182.00 kW		18170.65 kWh	
	TFOC w/o sail = 1468.63 L Emission w/o sail = 4573.30 kg				TFOC w/o sail = 4477.77 L Emission w/o sail = 13943.77 kg			
	Power Sail (kW)	TFOC w/Sail (L)	Emission (kg)	Reduction (%)	Power Sail (kW)	TFOC w/Sail (L)	Emission (kg)	Reduction (%)
Jan	3.69	1360.69	4169.82	8.82	7.50	4293.28	13369.27	4.12
Feb	3.07	1395.45	4237.18	7.35	6.44	4319.43	13450.72	3.54
Mar	2.08	1400.24	4345.43	4.98	4.51	4366.75	13598.07	2.48
Apr	1.95	1381.33	4360.35	4.66	3.52	4391.14	13674.00	1.93
May	2.48	1376.37	4301.47	5.94	3.96	4380.38	13640.51	2.17
Jun	2.63	1356.69	4286.01	6.28	4.07	4377.57	13631.75	2.24
Jul	3.19	1357.64	4224.74	7.62	4.87	4357.95	13570.66	2.68
Aug	3.16	1344.85	4227.70	7.56	5.00	4354.71	13560.57	2.75
Sep	3.52	1346.92	4187.87	8.43	5.99	4330.50	13485.18	3.29
Oct	3.46	1352.26	4194.32	8.29	6.23	4324.44	13466.29	3.42
Nov	3.31	1350.60	4210.93	7.92	6.19	4325.45	13469.46	3.40
Dec	3.36	1360.69	4205.77	8.04	6.73	4312.26	13428.37	3.70

The two speed points were selected to evaluate propulsion efficiency under varying sea conditions. Mathematical modeling shows that integrating sail technology can generate an effective thrust of 5.26 kW, improving operational economy with estimated fuel savings of 68.37 liters per voyage. Validation using Equation 10 confirms fluctuations in efficiency and emission reductions, yet both peak and minimum values follow a consistent pattern along the route, indicating strong seasonal influence on wind energy availability.

Based on Table 4, Route 1 consistently achieves the highest propulsion efficiency with an arc-shaped airfoil, especially at 7 knots, where emission reductions exceed 10% in several months and peak at 12.59% (July) and 12.19% (August). The system maintains efficiency above 6% annually, with trends governed by the Asian–Australian monsoon. During the East Monsoon (June–August), stable and stronger winds enhance aerodynamic performance, while at 10 knots efficiency decreases to 3–6% due to higher resistance and changes in apparent wind angles. Referring to Table 5, Route 2 shows greater variability. At 7 knots, efficiency peaks at 8.82% (January) and 8.43% (September), generally ranging from 6–8%, lower than Route 1 but still positive. At 10 knots, efficiency declines to 2–4%, with a maximum of 4.12% in January, likely due to differing wind and weather conditions along the longer route.

Table 6. Efficiency Results on Route 3 with Arc-shaped Sail

ROUTE 3 (839.07 NM)								
Arc Shaped								
Months	7 Knot (119.87 hr)				10 Knot (83.91 hr)			
	41.79 kW		5008.72 kWh		182.00 kW		15271.31 kWh	
	TFOC w/o sail = 1234.29 L Emission w/o sail = 3843.58 kg				TFOC w/o sail = 3763.29 L Emission w/o sail = 11718.88 kg			
	Power Sail (kW)	TFOC w/Sail (L)	Emission (kg)	Reduction (%)	Power Sail (kW)	TFOC w/Sail (L)	Emission (kg)	Reduction (%)
Jan	4.26	1108.51	3451.89	10.19	8.56	3586.22	11167.48	4.71
Feb	3.67	1125.78	3505.68	8.79	7.57	3606.83	11231.66	4.16
Mar	2.56	1158.66	3608.06	6.13	5.66	3646.26	11354.46	3.11
Apr	2.85	1150.26	3581.89	6.81	5.73	3644.87	11350.13	3.15
May	3.39	1134.20	3531.91	8.11	6.24	3634.23	11316.99	3.43
Jun	3.56	1129.03	3515.81	8.53	6.38	3631.40	11308.17	3.50
Jul	4.18	1110.83	3459.13	10.00	7.49	3608.35	11236.41	4.12
Aug	4.22	1109.67	3455.52	10.10	7.81	3601.89	11216.27	4.29
Sep	4.86	1090.85	3396.91	11.62	9.27	3571.67	11122.17	5.09
Oct	4.95	1088.00	3388.03	11.85	9.63	3564.21	11098.95	5.29
Nov	4.66	1096.62	3414.87	11.15	9.25	3571.95	11123.06	5.08
Dec	4.26	1108.61	3452.22	10.18	8.66	3584.15	11161.03	4.76

Table 7. Efficiency Results on Route 1 with Naca 0012 Sail

ROUTE 1 (369.14 NM)								
Naca 0012								
Months	7 Knot (52.73 hr)				10 Knot (36.91 hr)			
	41.79 kW		2203.50 kWh		182.00 kW		6718.35 kWh	
	TFOC w/o sail = 543.00 L Emission w/o sail = 1690.92 kg				TFOC w/o sail = 1655.59 L Emission w/o sail = 5155.52 kg			
	Power Sail (kW)	TFOC w/Sail (L)	Emission (kg)	Reduction (%)	Power Sail (kW)	TFOC w/Sail (L)	Emission (kg)	Reduction (%)
Jan	2.12	515.50	1605.26	5.07	4.29	1616.60	5034.10	2.36
Feb	1.80	519.65	1618.19	4.30	3.75	1621.46	5049.21	2.06
Mar	0.99	530.19	1651.01	2.36	2.52	1632.68	5084.16	1.38
Apr	1.62	521.97	1625.42	3.87	3.44	1624.33	5058.16	1.89
May	2.66	508.40	1583.16	6.37	4.93	1610.75	5015.88	2.71
Jun	3.10	502.77	1565.62	7.41	5.57	1604.95	4997.80	3.06
Jul	3.49	497.71	1549.86	8.34	6.26	1598.62	4978.11	3.44
Aug	3.38	499.15	1554.34	8.08	6.22	1599.03	4979.37	3.42
Sep	3.04	503.53	1568.00	7.27	5.93	1601.64	4987.50	3.26
Oct	2.56	509.81	1587.54	6.11	5.26	1607.76	5006.56	2.89
Nov	2.16	514.91	1603.42	5.17	4.64	1613.44	5024.24	2.55
Dec	1.72	520.65	1621.31	4.12	3.84	1620.64	5046.67	2.11

Based on Table 6, Route 3 shows the most consistent monthly efficiency among routes using an arc-shaped airfoil. At 7 knots, emission reductions range from 6% to 10%, peaking at 11.85% (October) and 11.62% (September). Despite being longer than Route 1, sails remain effective at this speed. At 10 knots, efficiency remains stable at 3–5% annually, with peaks of 5.29% (October) and 5.08% (September).

Referring to Table 7, Route 1 with a NACA 0012 airfoil shows lower efficiency than the arc-shaped type. At 7 knots, reductions peak at 8.34% (July) and 8.08% (August), reflecting favorable wind conditions. However, at 10 knots, efficiency declines, with maximum values of 3.44% (July) and 3.42% (August), indicating better performance at lower ship speeds.

Table 8. Efficiency Results on Route 2 with NACA 0012 Sail

ROUTE 2 (998.37 NM)								
NACA 0012								
Months	7 Knot (142.62 hr)				10 Knot (99.84 hr)			
	41.79 kW		5959.64 kWh		182.00 kW		18170.65 kWh	
	TFOC w/o sail = 1468.63 L Emission w/o sail = 4573.30 kg				TFOC w/o sail = 4477.77 L Emission w/o sail = 13943.77 kg			
	Power Sail (kW)	TFOC w/Sail (L)	Emission (kg)	Reduction (%)	Power Sail (kW)	TFOC w/Sail (L)	Emission (kg)	Reduction (%)
Jan	2.44	1382.78	4305.98	5.85	4.97	4355.54	13563.15	2.73
Feb	2.04	1397.11	4350.61	4.87	4.26	4372.87	13617.10	2.34
Mar	1.38	1420.15	4422.33	3.30	2.99	4404.22	13714.73	1.64
Apr	1.29	1423.32	4432.22	3.09	2.33	4420.37	13765.04	1.28
May	1.65	1410.79	4393.21	3.94	2.62	4413.25	13742.85	1.44
Jun	1.74	1407.50	4382.96	4.16	2.70	4411.38	13737.05	1.48
Jul	2.11	1394.47	4342.37	5.05	3.23	4398.38	13696.57	1.77
Aug	2.09	1395.10	4344.33	5.01	3.31	4396.24	13689.89	1.82
Sep	2.33	1386.62	4317.94	5.58	3.97	4380.20	13639.94	2.18
Oct	2.29	1387.99	4322.21	5.49	4.13	4376.18	13627.42	2.27
Nov	2.19	1391.53	4333.22	5.25	4.10	4376.85	13629.52	2.25
Dec	2.23	1390.43	4329.80	5.32	4.46	4368.11	13602.30	2.45

Sail performance on Route 2 (Table 8) shows lower efficiency than on Route 1 (Table 7), reflecting variations in operational conditions along the longer route. At a speed of 7 knots, the highest efficiency was recorded in January, the beginning of the year, with a reduction of 5.85%. However, this figure remains lower than the peak performance on Route 1. At a speed of 10 knots, efficiency again declined substantially, with reduction values generally in the range of 1% to 2%, and peak efficiency only reaching 2.73% in January.

Table 9. Efficiency Results on Route 3 with NACA 0012 Sail

ROUTE 3 (839.07 NM)								
NACA 0012								
Months	7 Knot (119.87 hr)				10 Knot (83.91 hr)			
	41.79 kW		5008.72 kWh		182.00 kW		15271.31 kWh	
	TFOC w/o sail = 1234.29 L Emission w/o sail = 3843.58 kg				TFOC w/o sail = 3763.29 L Emission w/o sail = 11718.88 kg			
	Power Sail (kW)	TFOC w/Sail (L)	Emission (kg)	Reduction (%)	Power Sail (kW)	TFOC w/Sail (L)	Emission (kg)	Reduction (%)
Jan	2.82	1150.96	3584.07	6.75	5.67	3645.97	11353.56	3.12
Feb	2.43	1162.40	3619.71	5.82	5.01	3659.63	11396.08	2.75
Mar	1.70	1184.18	3687.54	4.06	3.75	3685.75	11477.44	2.06
Apr	1.89	1178.61	3670.21	4.51	3.79	3684.83	11474.57	2.08
May	2.25	1167.98	3637.09	5.37	4.14	3677.78	11452.61	2.27
Jun	2.36	1164.55	3626.42	5.65	4.23	3675.91	11446.77	2.32
Jul	2.77	1152.50	3588.87	6.63	4.96	3660.64	11399.23	2.73
Aug	2.80	1151.73	3586.48	6.69	5.17	3656.35	11385.89	2.84
Sep	3.22	1139.26	3547.65	7.70	6.14	3636.33	11323.54	3.37
Oct	3.28	1137.37	3541.76	7.85	6.38	3631.39	11308.16	3.50
Nov	3.09	1143.08	3559.55	7.39	6.13	3636.52	11324.13	3.36
Dec	2.82	1151.03	3584.29	6.75	5.74	3644.60	11349.28	3.15

Route 3 shows the efficiency between Routes 1 and 2. At a speed of 7 knots, sail performance shows relatively good stability, with the highest efficiency recorded in October at 7.85% and September at 7.70%. This pattern indicates that conditions on Route 3 in certain months are also highly conducive to sail use. As with other routes, at 10 knots, efficiency decreases dramatically, by 2% to 3.5%, and the highest efficiency is recorded in October at 3.50%.

Table 10. Efficiency Results on Route 1 with NACA 0015 Sail

ROUTE 1 (369.14 NM)								
NACA 0015								
Months	7 Knot (52.73 hr)				10 Knot (36.91 hr)			
	41.79 kW		2203.50 kWh		182.00 kW		6718.35 kWh	
	TFOC w/o sail = 543.00 L Emission w/o sail = 1690.92 kg				TFOC w/o sail = 1655.59 L Emission w/o sail = 5155.52 kg			
	Power Sail (kW)	TFOC w/Sail (L)	Emission (kg)	Reduction (%)	Power Sail (kW)	TFOC w/Sail (L)	Emission (kg)	Reduction (%)
Jan	1.89	518.45	1614.46	4.52	3.83	1620.79	5047.14	2.10
Feb	1.60	522.16	1626.00	3.84	3.35	1625.12	5060.63	1.84
Mar	0.88	531.57	1655.30	2.11	2.25	1635.14	5091.83	1.24
Apr	1.45	524.23	1632.46	3.46	3.07	1627.69	5068.62	1.69
May	2.38	512.12	1594.73	5.69	4.40	1615.57	5030.88	2.42
Jun	2.76	507.09	1579.08	6.61	4.97	1610.39	5014.75	2.73
Jul	3.11	502.57	1565.01	7.45	5.59	1604.74	4997.16	3.07
Aug	3.01	503.86	1569.01	7.21	5.55	1605.11	4998.30	3.05
Sep	2.71	507.77	1581.20	6.49	5.29	1607.43	5005.55	2.91
Oct	2.28	513.37	1598.65	5.46	4.69	1612.90	5022.57	2.58
Nov	1.93	517.92	1612.82	4.62	4.14	1617.96	5038.34	2.27
Dec	1.54	523.05	1628.79	3.67	3.43	1624.39	5058.36	1.88

On Route 1 in Table 10, the NACA 0015 airfoil achieved the highest efficiency among all observed routes. At 7 knots, emission reductions peaked in July (7.45%) and June (6.61%), with a general efficiency range of 3–7%. Conversely, at 10 knots, efficiency dropped significantly to a maximum of only 3.07% (July), maintaining a stable range between 1–3%.

Table 11. Efficiency Results on Route 2 with NACA 0015 Sail

ROUTE 2 (998.37 NM)								
NACA 0015								
Months	7 Knot (142.62 hr)				10 Knot (99.84 hr)			
	41.79 kW		5959.64 kWh		182.00 kW		18170.65 kWh	
	TFOC w/o sail = 1468.63 L Emission w/o sail = 4573.30 kg				TFOC w/o sail = 4477.77 L Emission w/o sail = 13943.77 kg			
	Power Sail (kW)	TFOC w/Sail (L)	Emission (kg)	Reduction (%)	Power Sail (kW)	TFOC w/Sail (L)	Emission (kg)	Reduction (%)
Jan	2.18	1392.00	4334.70	5.22	4.43	4368.67	13604.04	2.44
Feb	1.82	1404.80	4374.53	4.35	3.81	4384.14	13652.20	2.09
Mar	1.23	1425.35	4438.55	2.95	2.67	4412.12	13739.34	1.47
Apr	1.15	1428.19	4447.37	2.75	2.08	4426.54	13784.24	1.14
May	1.47	1417.01	4412.55	3.51	2.34	4420.18	13764.44	1.29
Jun	1.55	1414.07	4403.41	3.71	2.41	4418.51	13759.25	1.32
Jul	1.88	1402.43	4367.18	4.51	2.88	4406.91	13723.12	1.58
Aug	1.87	1403.00	4368.93	4.47	2.96	4405.00	13717.16	1.63
Sep	2.08	1395.43	4345.38	4.98	3.54	4390.68	13672.58	1.94
Oct	2.05	1396.66	4349.19	4.90	3.69	4387.09	13661.41	2.03
Nov	1.96	1399.81	4359.01	4.69	3.66	4387.70	13663.28	2.01
Dec	1.99	1398.83	4355.96	4.75	3.98	4379.89	13638.98	2.19

Sail performance on Route 2 in Table 11 is the lowest of the three routes. At a speed of 7 knots, the highest efficiency was recorded in January at 5.22%. During the rest of the year, efficiency was in the lower range of 2-5%. At 10 knots, emission-reduction efficiency is minimal, with most data below 2%. The highest values were recorded at 2.44% in January and 2.19% in December.

Table 12. Efficiency Results on Route 3 with NACA 0015 Sail

ROUTE 3 (839.07 NM)								
NACA 0015								
Months	7 Knot (119.87 hr)				10 Knot (83.91 hr)			
	41.79 kW		5008.72 kWh		182.00 kW		15271.31 kWh	
	TFOC w/o sail = 1234.29 L Emission w/o sail = 3843.58 kg				TFOC w/o sail = 3763.29 L Emission w/o sail = 11718.88 kg			
	Power Sail (kW)	TFOC w/Sail (L)	Emission (kg)	Reduction (%)	Power Sail (kW)	TFOC w/Sail (L)	Emission (kg)	Reduction (%)
Jan	2.52	1159.91	3611.95	6.03	5.06	3658.58	11392.80	2.78
Feb	2.17	1170.12	3643.76	5.20	4.48	3670.76	11430.76	2.46
Mar	1.51	1189.57	3704.31	3.62	3.35	3694.08	11503.38	1.84
Apr	1.68	1184.60	3688.83	4.03	3.39	3693.26	11500.82	1.86
May	2.00	1175.10	3659.27	4.80	3.69	3686.97	11481.22	2.03
Jun	2.11	1172.05	3649.75	5.04	3.77	3685.29	11476.00	2.07
Jul	2.47	1161.28	3616.23	5.92	4.43	3671.67	11433.57	2.43
Aug	2.50	1160.60	3614.10	5.97	4.62	3667.84	11421.66	2.54
Sep	2.87	1149.47	3579.44	6.87	5.48	3649.97	11366.01	3.01
Oct	2.93	1147.78	3574.19	7.01	5.69	3645.56	11352.28	3.13
Nov	2.76	1152.88	3590.06	6.60	5.47	3650.14	11366.54	3.01
Dec	2.52	1159.97	3612.15	6.02	5.12	3657.35	11388.99	2.82

Route 3 (Table 12) with NACA 0015 shows higher efficiency than Route 2. At 7 knots, peak efficiency occurs in October (7.01%) and September (6.87%), with averages of 3–7%, indicating reliable performance. At 10 knots, efficiency declines but savings persist, peaking at 3.13% (October) and 3.01% (September). Overall, efficiency is consistently higher at lower power levels. This is driven by changes in relative wind affecting sail thrust and by lower power demand at 7 knots, where the sail's contribution becomes more significant than at higher speeds. [28].

In applying WASP technology, wing geometry selection must consider local wind characteristics shaped by the Asia Australia monsoon. As these variations also alter ocean energy distribution, the wing structure must be robust enough to withstand extreme conditions, ensuring vessel integrity and reducing maritime risk [29].

CONCLUSION

The integration of Wind-Assisted Ship Propulsion (WASP) with an A*-based routing framework significantly improves vessel efficiency, particularly with arc-shaped sails. These sails outperform symmetrical NACA 0012 and NACA 0015 profiles due to higher lift, generating greater auxiliary thrust. Performance is strongly speed-dependent, with optimal results at lower speeds (7 knots), where wind contribution is more dominant. By combining real-time weather data with sail force matrices, this study offers a scalable approach to support IMO decarbonization targets, especially in archipelagic regions like Indonesia. Future work should focus on wing-sail structural integrity and the integration of machine learning to improve route prediction under dynamic sea conditions.

ACKNOWLEDGEMENT

The authors would like to thank their gratitude to the Department of Naval Engineering at Universitas Pembangunan Nasional Veteran Jakarta, Indonesia, for providing the necessary academic support throughout this research. The MBKM (Merdeka Belajar-Kampus Merdeka) program at the Hydrodynamics Technology Research Center (PRTH) of the National Research and Innovation Agency (BRIN), Surabaya, Indonesia. Appreciation is also extended to the Ministry of Marine Affairs and Fisheries (KKP) Indonesia for providing fishing vessel route data.

REFERENCES

[1] S. Bali, S. Thangalakshmi, and R. Balaji, "Renewable Energy Options for Seaports," *Ocean. Conf. Rec.*, no. January, 2022, doi: 10.1109/OCEANSChennai45887.2022.9775323.

[2] IMO, "ANNEX 11 MEPC.304(72) - Initial IMO strategy on reduction of GHG emissions from ships," *IMO Publ.*, vol. 304, no. April, pp. 1–11, 2018, [Online]. Available: http://www.imo.org/en/KnowledgeCentre/IndexofIMOResolutions/Marine-Environment-Protection-Committee-%28MEPC%29/Documents/MEPC.304%2872%29.pdf

[3] Suardi, D. Suanggana, and B. Said, "Biodiesel Potentials of Waste Cooking Oil (WCO): Production, Content of Fuel Properties, and Effects on Engine Performance", IJMEIR, vol. 8, no. 2, pp. 213–221, Jul. 2025. doi: https://doi.org/10.12962/j25481479.v8i2

[4] Suardi, M. Purwanto, A. Y. Kyaw, W. Setiawan, M. U. Pawara, and Alfawan, "Biodiesel Production from POME (Palm Oil Mill Effluent) and Effects on Diesel Engine Perfor-mance", IJMEIR, vol. 7, no. 4, pp. 292–299, Jul. 2025. doi: https://doi.org/10.12962/j25481479.v7i4

[5] M. D. Hussain, M. S. Tuhin, S. Kabir, and O. M. Amin, "Numerical investigation of the stability and power prediction of a sail based wind propulsion system for a cargo ship," *AIP Conf. Proc.*, vol. 1980, no. July, 2018, doi: 10.1063/1.5044374.

[6] D. Li, Y. Zhang, P. Li, J. Dai, and G. Li, "Aerodynamic performance of a new double-flap wing sail," *Polish Marit. Res.*, vol. 26, no. 4, pp. 61–68, 2019, doi: 10.2478/pomr-2019-0067.

[7] T. P. V. Zis, H. N. Psaraftis, and L. Ding, "Ship weather routing: A taxonomy and survey," *Ocean Eng.*, vol. 213, no. March, p. 107697, 2020, doi: 10.1016/j.oceaneng.2020.107697.

[8] W. Sun, S. Tang, X. Liu, S. Zhou, and J. Wei, "An Improved Ship Weather Routing Framework for CII Reduction Accounting for Wind-Assisted Rotors," *J. Mar. Sci. Eng.*, vol. 10, no. 12, 2022, doi: 10.3390/jmse10121979.

[9] K. Wang *et al.*, "Joint energy consumption optimization method for wing-diesel engine-powered hybrid ships towards a more energy-efficient shipping," *Energy*, vol. 245, p. 123155, 2022, doi: 10.1016/j.energy.2022.123155.

[10] C. Guzelbulut, T. Badalotti, and K. Suzuki, "Optimization techniques for the design of crescent-shaped hard sails for wind-assisted ship propulsion," *Ocean Eng.*, vol. 312, no. P1, p. 119142, 2024, doi: 10.1016/j.oceaneng.2024.119142.

[11] M. N. Nyanya, H. B. Vu, A. Schönborn, and A. I. Ölçer, "Wind and solar assisted ship propulsion

optimisation and its application to a bulk carrier," *Sustain. Energy Technol. Assessments*, vol. 47, no. September 2020, 2021, doi: 10.1016/j.seta.2021.101397.

[12] I. Göv, M. Hanifi Doğru, İ. Göv, and M. H. Doğru, "Aerodynamic Optimization of Naca 0012 Airfoil," *Int. J. Energy Eng. Sci.*, vol. 2020, no. 2, pp. 146–155, 2020, [Online]. Available: https://www.researchgate.net/publication/374004748

[13] R. R. I., Uddin, Islam, and Rokunuzzaman, "Comparison of Aerodynamics Characteristics of Naca 0015 & Naca 4415 Aerofoil Blade," *Int. J. Res. -GRANTHAALAYAH*, vol. 5, no. 11, pp. 187–197, 2017, doi: 10.29121/granthaalayah.v5.i11.2017.2346.

[14] Y. Wang, X. Zhang, S. Lin, Z. Qiang, J. Hao, and Y. Qiu, "Analysis on the Development of Wind-assisted Ship Propulsion Technology and Contribution to Emission Reduction," in *IOP Conference Series: Earth and Environmental Science*, IOP Publishing Ltd, Jan. 2022. doi: 10.1088/1755-1315/966/1/012012.

[15] American Bureau of Shipping, *WIND PROPULSION TECHNOLOGIES*. 2025.

[16] J. Mason, A. Larkin, S. Bullock, N. van der Kolk, and J. F. Broderick, "Quantifying voyage optimisation with wind propulsion for short-term CO_2 mitigation in shipping," *Ocean Eng.*, vol. 289, no. November, 2023, doi: 10.1016/j.oceaneng.2023.116065.

[17] M. Il Roh, "Determination of an economical shipping route considering the effects of sea state for lower fuel consumption," *Int. J. Nav. Archit. Ocean Eng.*, vol. 5, no. 2, pp. 246–262, 2013, doi: 10.2478/ijnaoe-2013-0130.

[18] R. W. Reynolds, T. M. Smith, C. Liu, D. B. Chelton, K. S. Casey, and M. G. Schlax, "Daily high-resolution-blended analyses for sea surface temperature," *J. Clim.*, vol. 20, no. 22, pp. 5473–5496, 2007, doi: 10.1175/2007JCLI1824.1.

[19] ITTC, "Report of the Wind Powered and Wind Assisted Ships Committee," 2024.

[20] C. T. Riccardo De Lauretis, Leonidas Ntziachristos, "International maritime navigation, international inland navigation, national navigation (shipping), national fishing, military (shipping), and recreational boats," in *EMEP/EEA air pollutant emission inventory guidebook 2023*, 2023.

[21] R. F. Fadillah and F. A. Ayub, "Estimation of daily CO_2 emission generated by container ship classified by ClassNK," *IOP Conf. Ser. Earth Environ. Sci.*, vol. 1454, no. 1, 2025, doi: 10.1088/1755-1315/1454/1/012036.

[22] R. Zhang *et al.*, "Numerical investigation on the effects of heel on the aerodynamic performance of wing sails," *Ocean Eng.*, vol. 305, no. February, p. 117897, 2024, doi: 10.1016/j.oceaneng.2024.117897.

[23] P. Sachs, G., Bussotti, "In: Giannessi, F., Maugeri, A. (eds), Application of Optimal Control Theory to Dynamic Soaring of Seabirds. Variational Analysis and Applications. Nonconvex Optimization and Its Applications, vol 79.," in *Variational Analysis and Applications. Nonconve*, Springer, 2005. doi: https://doi.org/10.1007/0-387-24276-7_57.

[24] C. Li, H. Wang, and P. Sun, "Study on the Influence of Gradient Wind on the Aerodynamic Characteristics of a Two-Element Wingsail for Ship-Assisted Propulsion," *J. Mar. Sci. Eng.*, vol. 11, no. 1, 2023, doi: 10.3390/jmse11010134.

[25] Y. Li, Y. Zhang, and F. Zhu, "Minimal time route for wind-assisted ships," *Mar. Technol. Soc. J.*, vol. 48, no. 3, pp. 115–124, 2014, doi: 10.4031/MTSJ.48.3.2.

[26] A. M. A. Rufatin, A. Yananto, and W. W. Pandoe, "Jurnal Teknologi Lingkungan Karakteristik Angin Wilayah Pesisir Utara Pulau Jawa Berdasarkan Variabilitas Monsun Wind Characteristics of the North Coastal Region of Java Island According to Monsoon Variability," vol. 25, no. 1, pp. 20–30, 2024, doi: https://doi.org/10.55981/jtl.2024.2039.

[27] M. F. Rahmat *et al.*, "Assessment of Wave Characteristics in National Water Borders for Tactical Vessel Analysis and Maritime Security," vol. 04, no. 01, pp. 14–27, 2026, doi: https://doi.org/10.35718/ismatech.v4i1.8481963.

[28] R. Ma *et al.*, "Evaluation Method for Energy Saving of Sail-Assisted Ship Based on Wind Resource Analysis of Typical Route," *J. Mar. Sci. Eng.*, vol. 11, no. 4, 2023, doi: 10.3390/jmse11040789.

[29] E. Pramudya Imawan Santosa, Mochamad Zaed Yuliadi, Achmad Fajar, Suardi, Yulia Ayu Nastiti and Pranatal, "Ship Design Based on Extreme Waves," vol. 03, no. 01, pp. 60–66, 2025, doi: https://doi.org/10.35718/ismatech.v3i1.1353.